1760 nm Multi-Watt Broadband PM CW and Pulsed Tm-Doped Fiber Amplifier

Wiktor Walasik, *Member, IEEE*, Robert E. Tench, *Senior Member, IEEE*, Gustavo Rivas, Jean-Marc Delavaux, *Senior Member, IEEE*, and Ian Farley

***Abstract*—We report the performance of CW and pulsed single-clad PM Tm-doped fiber amplifiers optimized for the wavelength band from 1760 to 1960 nm. For the CW regime, we have achieved output power levels as high as 3 W with a two-stage TDFA designed for operation at 1760 nm. Simulations indicate that this 3 W output power extends from 1760 nm to 1960 nm. OSNR values >55 dB in 0.1 nm are experimentally measured for the optimized two-stage TDFA. In the pulsed regime, we studied the performance of the amplifier with 50–100 ns input pulses and repetition rates from 100 kHz to 1 MHz. We studied in detail the evolution of the output pulse shape, first with square input, and then with shaped input pulses using an arbitrary waveform generator that resulted in an optimized square output pulse shape. Average output powers of 2 W, peak output powers of 20 W (10% duty cycle), and pulse energies of 1.6 μJ were achieved.**

***Index Terms*—1760 nm, near-infrared, optical amplifiers, optical fiber devices, polarization maintaining fiber amplifiers, thulium-doped fiber amplifiers.**

I. Introduction

RECENT Work in thulium-doped fiber amplifiers (TDFAs) demonstrates that these devices are capable of operation over a wide wavelength region spanning from 1630 to more than 2100 nm [1], [2], [3], [4], [5], [6], [7]. While conventional TDFAs typically span 1850–2000 nm [5], [6], [7], extended wavelength TDFAs using custom research Ge/Tm co-doped silica fibers operate at wavelengths as low as 1630 nm [1], [2], [3], [4]. TDFAs which readily access the 1730–1800 nm region are of particular interest because of rich molecular absorptions near 1730 and 1760 nm in CH_2 and other molecules that are significant for bio-photonics applications [8], [9], [10]. Also, both continuous wave (CW) and pulsed operation modes of the amplifier are quite important for mid-IR frequency generation, Raman soliton generation in conventional Si fibers, direct detection and coherent communications applications, and quantum computing applications at 1762 nm employing ^{133}Ba+ ions. [9], [10], [11], [12], [13], [14], [15], [29], [30].

Manuscript received 9 November 2022; revised 22 March 2023; accepted 18 April 2023. Date of publication 25 April 2023; date of current version 27 June 2023. *(Corresponding author: Robert E. Tench.)*

Wiktor Walasik, Robert E. Tench, Gustavo Rivas, and Jean-Marc Delavaux are with the Cybel LLC, Bethlehem, PA 18017 USA (e-mail: wiktor.walasik@cybel-llc.com; robert.tench@cybel-llc.com; gustavo.rivas@cybel-llc.com; jm@cybel-llc.com).

Ian Farley is with the Eblana Photonics Ltd., A96 A621 Dublin, Ireland (e-mail: ian.farley@eblanaphotonics.com).

Color versions of one or more figures in this article are available at https://doi.org/10.1109/JLT.2023.3269985.

Digital Object Identifier 10.1109/JLT.2023.3269985

A survey of the literature on Tm-doped fiber lasers and amplifiers in the 1620–1800 nm region indicates many recent significant technical advances.

For Tm-doped fiber lasers most have been realized with a hybrid fiber/bulk optics configuration. In 2006, Shen et al. reported laser operation from 1750–1900 nm with a maximum CW output power of 8 W [16]. In 2015, Daniel et al. described laser operation at 1726 nm with 12 W CW output power [2]. Also in 2015, Quan et al. presented results for laser operation at 1750 nm with 0.4 W CW output power using a volume Bragg grating [17]. In 2019, Burns et al. reported 47 W CW output from a laser at 1726 nm [18]. The only laser with an all-fiber configuration known to the authors was demonstrated by Zhang et al. in 2021 and delivered 1 W CW output power at 1720 nm [19]. All of these reported laser sources are non-polarization maintaining (non-PM) and do not incorporate optical isolators for feedback reduction.

However, it is well known that there are many significant technical differences between fiber lasers and fiber amplifiers. For TDFAs operating in the 1620–1800 nm region, only two low-power, all-fiber configurations have recently been demonstrated. In 2016, Li et al. presented a TDFA operating from 1700–1800 nm with 0.1 W CW output power [3]. In 2019, Chen et al. described a TDFA with 0.2 W CW output power and an operating wavelength range of 1620–1660 nm [4]. Both of these reported fiber amplifiers were non-PM and only the former had an output isolator. In [31] an 1807 nm TDFA is reported in simulations, but no experimental data are presented. In [32] a 2 W TDFA for 1762 nm is discussed, but no published simulations or experimental data are presented.

In this paper we propose and demonstrate a high-performance broadband PM TDFA operating from 1760–1960 nm that uses standard commercially available Tm-doped fibers [5], [6], [7], [15], has a fiber coupled output power as high as 3 W CW, exhibits more than 20 W of peak power in the pulsed regime, and incorporates optical isolators and circulators for suppression of the effects of reflection and feedback.

To our knowledge, this is the first demonstration of multi-Watt all-fiber single clad PM TDFA operation in the 1760–1960 nm wavelength region, and also the first report of ns pulsed single clad TDFA operation with a PM configuration.

The manuscript is organized as follows: Section II describes the experimental setup used for the CW experiments. Section III discusses the performance of a single-stage CW amplifier operating at 1760 nm, and Section IV covers the CW performance

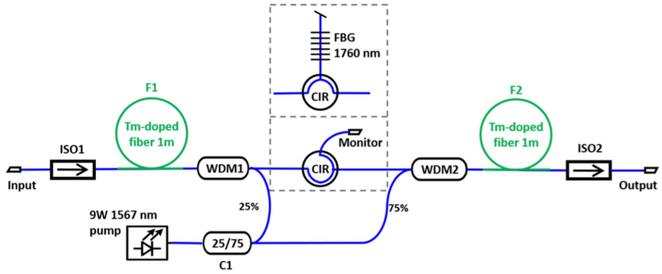

Fig. 1. Optical architecture of the two-stage PM 1760 nm TDFA.

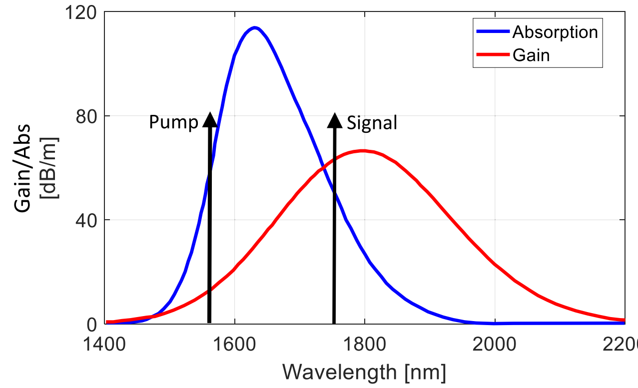

Fig. 2. Absorption and gain coefficients for the iXblue Tm-doped fiber.

of the two-stage TDFA. Section V presents the experimental results obtained while operating the TDFA as an ASE source. In Section VI, the pulsed performance of the two-stage TDFA is described. Finally, a discussion and conclusions are given in Sections VII and VIII.

II. Experimental Setup

Fig. 1 shows the configuration of the 1760 nm PM TDFA operated in a CW regime. This amplifier consists of a preamplifier stage followed by a booster stage. A 9-W 1567 nm fiber laser pump power (P_P) is split by a 75/25 passive coupler C1 to counter-pump (25%) the preamplifier stage and co-pump (75%) the booster stage via high-power PM fused fiber wavelength division multiplexers WDM1 and WDM2. Both amplifier stages use the same standard commercial 5 μm core diameter PM TDF (iXblue IXF-TDF-PM-5-125). The gain fibers F1 and F2 are both 1 m long. These lengths were determined by an initial simulation which indicated that second stage fiber coupled signal output powers $P_S > 3$ W could readily be achieved at the signal wavelength $\lambda_S = 1760$ nm, i.e., the lower limit of the targeted signal wavelength band, with input signal powers $P_{in} > 4$ mW (+6 dBm). The P_S of the first stage is measured at the output of circulator CIR.

In the current experiments, a PM circulator CIR was used as an interstage isolator. The third port of the isolator was used as a monitor for the backward emitted light from the booster stage. This will be replaced in the future by an interstage filter composed of a circulator CIR (note different orientation of the circulator outputs in Fig. 1) and a narrow-band fiber Bragg grating (FBG) reflector. Both the input and output of the amplifier are protected from optical reflections by the PM isolators ISO1 and ISO2, respectively.

The performance of the TDFA was simulated using an in-house software program and the absorption and gain coefficients for the iXblue IXF-TDF-PM-5-125 active fiber shown in Fig. 2 [5], [6], [7]. The model employed was a simplified three level Giles model [20], [21] in which the relevant rate equations and propagation equations were solved with a stiff solver and the fourth-order Runge-Kutta technique. The wavelength independent saturation parameter for the fiber is 1.57×10^{18} m^{-1} s^{-1} [5], [6], [7], [20], [21]. Other physical parameters of the fiber are listed in Table I. The simulated group velocity dispersion of the fiber is -26 ps^2 km^{-1} at 1760 nm and -47 ps^2 km^{-1} at 1975 nm.

TABLE I
Key Physical Parameters for IXF-TDF-PM-5-125 Ixblue Tm-Doped PM Fiber

Parameter	Value	Unit
Core Diameter	4.5 ±0.5	µm
Core NA	0.25	-
3F4 Lifetime	0.750	ms
Absorption, @ 1550 nm	45.3	dB/m
Absorption, @ 1760 nm	46.1	dB/m
Absorption, @ 1952 nm	1.23	dB/m
Gain, @ 1550 nm	11.3	dB/m
Gain, @1760 nm	64.5	dB/m
Gain, @ 1952 nm	34.8	dB/m
Background loss	200	dB/km
Birefringence	>2E-04	-
Number Density	7.40E+25	m^{-3}

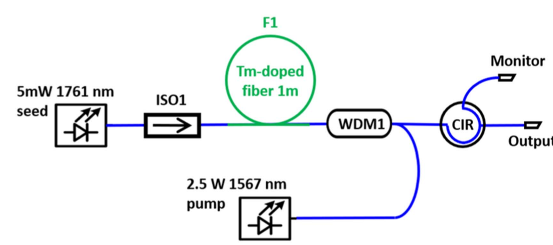

Fig. 3. Optical architecture of the PM 1760 nm TDFA preamplifier.

We note that typical splice losses between the PM Tm-doped fiber and a matching passive PM fiber are 0.1 dB or less. We also note that at the 1760 nm signal wavelength of interest, the fiber gain parameter is 64.5 dB/m and the absorption parameter is 46.1 dB/m as illustrated in Fig. 2. Since these values are close to one another in magnitude, and since the absorption coefficient increases rapidly with decreasing signal wavelength from this point, we observe that the expected low wavelength cutoff for the operating band of the amplifier is expected to be around 1740 to 1750 nm. This observation will be more fully quantified in Section IV below.

III. CW Performance of a Single-Stage TDFA

Fig. 3 shows the architecture of the preamplifier stage of the TDFA. The performance of this stage was tested with a discrete

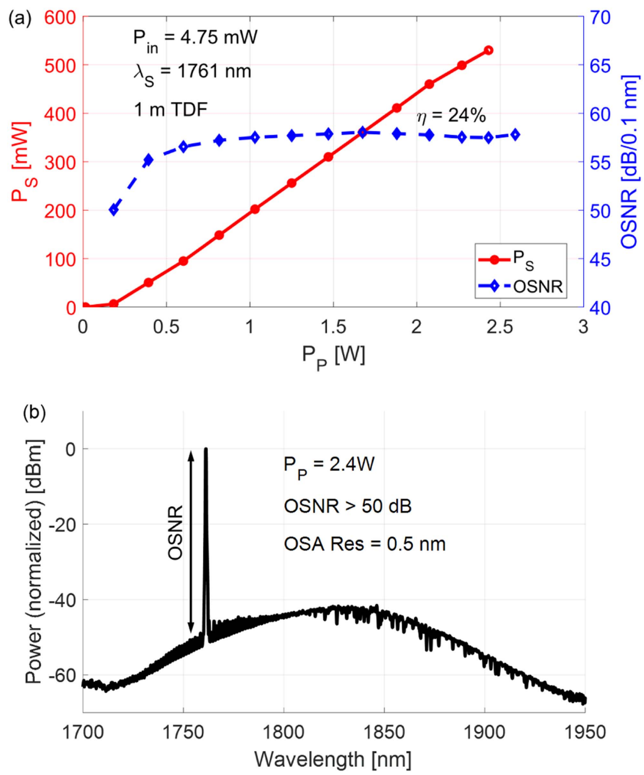

Fig. 4. (a) Output power (left axis) and OSNR (right axis) of the preamplifier TDFA vs 1567 nm pump power for 4.75 mW of CW input signal at 1761 nm. (b) Output spectrum of the preamplifier TDFA.

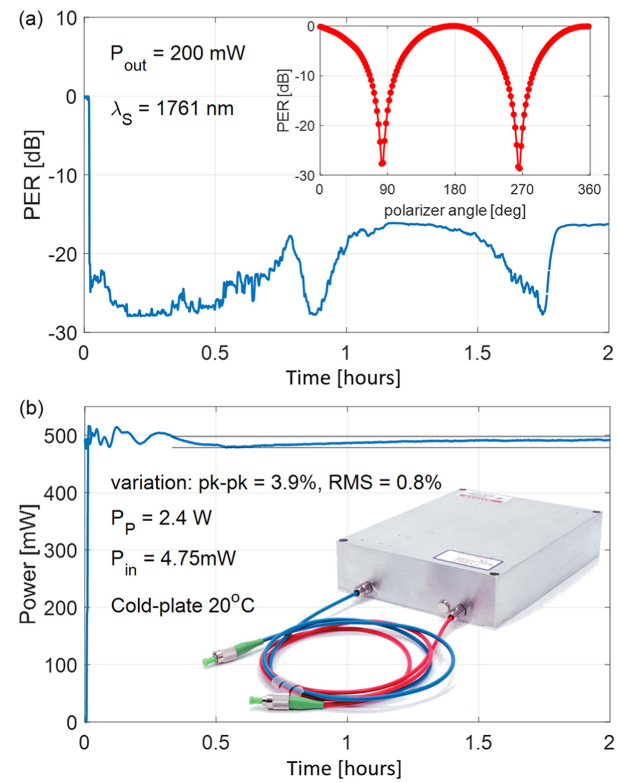

Fig. 5. (a) Polarization stability of preamplifier stage measured over the period of 2 hours. The inset shows the PER visibility curve. (b) Output power stability measured over 2 hours. The inset shows the amplifier package.

mode (DM) packaged seed laser from Eblana with 4.75 mW fiber coupled output power, a wavelength of 1761 nm, and a linewidth of <2 MHz. Up to 2.5 W of P_P at 1567 nm was available from a high-power fiber laser source. ISO1, CIR, F1, and WDM1 are the same as the components in the amplifier of Fig. 1. The signal channel insertion losses are: 2.0 dB for ISO1, and 2.0 dB for the input to the output port of the circulator, and 0.9 dB for the WDM. The pump channel loss in the WDM is 0.2 dB.

The 1760 nm preamplifier output power (P_S) and the OSNR as a function of 1567 nm P_P are plotted in Fig. 4(a). Here we see a linear dependence of P_S versus P_P with an optical-to-optical conversion efficiency slope (η) of 24%. The output power P_S is 520 mW at a maximum P_P of 2.4 W. As shown in Fig. 4(b), the measured OSNR at the signal wavelength is greater than 55 dB in 0.1 nm for P_P above 0.5 W, and was measured with the optical spectrum analyzer (Yokogawa AQ6375B) with resolution of 0.5 nm (−3-dB bandwidth). Also, we derive that P_S contains more than 98.5% of the total output power (signal + ASE). When considering the OSNR with to respect to the peak amplified spontaneous emission (ASE) power, its value is 47 dB in 0.1 nm, which is still pretty large.

In small signal regime, 30 dB of fiber-to-fiber gain (G) was measured for a −18 dBm of P_{in} and $P_P = 1$ W. The corresponding simulated small signal noise figure (NF) is 6.3 dB. For a P_{in} of 0 dBm the G value was reduced to 25 dB and 22 dB for 1.9 W and 1.0 W of P_P, respectively. However, we observed the occurrence of self-lasing in the amplifier for $P_P > 1.9$ W, and for $P_{in} < -4$ dBm. Overall, these results confirmed that this single preamplifier stage can deliver large G in the small signal regime and Watt-level output powers in the saturation regime at 1760 nm.

Fig. 5(a) shows the measured stability of the output polarization for the preamplifier over a time interval of two hours. The polarization extinction ratio (PER) remains above 17 dB during this time and it is determined by the performance of the circulator CIR whose specified polarization extinction ratio is ≥17 dB. The inset in Fig. 5(a) plots the PER visibility curve measured by transmitting the output signal through a rotating linear polarizer and reveals 28 dB of PER contrast. Measurements of the P_S stability over a time interval of two hours, given in Fig. 6(b), indicate that the peak-to-peak output power variation is 3.9% and the root-mean-square (RMS) variation is 0.8%, after 20 minutes of stabilization. The high preamplifier output power and high polarization stability are advantageous features in the operation of the full two-stage TDFA, which is discussed in the next section.

Our Tm-doped fiber amplifier assembly has dimensions of 200 × 150 × 43 mm^3 and is shown in the inset of Fig. 5(b). It is pumped by a passively cooled semiconductor laser source, has an operating temperature range of −20 to +40 C, and is suitable for immediate integration into existing laboratory setups and photonic equipment. The input and output fiber pigtails are Coherent/Nufern PM1950 fiber cables terminated with FC/APC connectors.

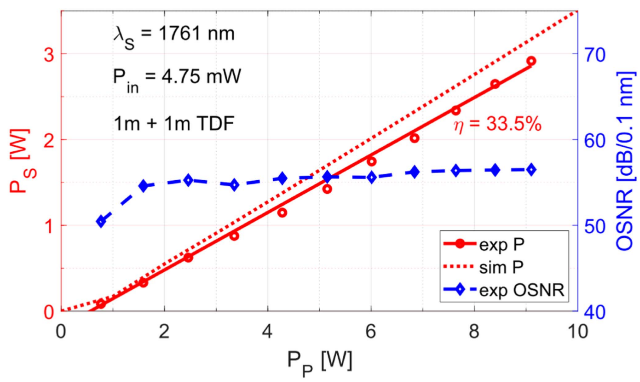

Fig. 6. Experimentally measured (red, solid line) and simulated (red, dashed line) output power (left axis) and OSNR (right axis, blue, dashed) of the two-stage TDFA vs 1567 nm pump power for 4.75 mW of CW input signal at 1761 nm.

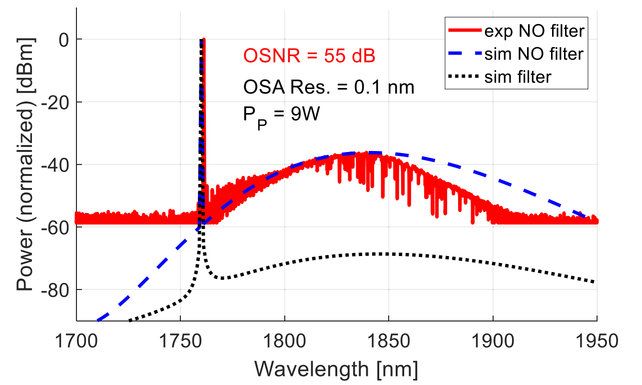

Fig. 7. Output spectra of the TDFA measured with 0.1 nm resolution: experimentally measured (red) and simulated (blue) spectra with inter-stage isolator are compared with the simulated spectrum with an interstage filter (black).

IV. CW Performance of the Two-Stage TDFA

Fig. 6 shows the experimental and simulation results obtained with the PM two-stage TDFA shown in Fig. 1. The insertion losses of the WDM2 were 0.3 and 0.4 dB at the signal and pump wavelengths, respectively. The insertion loss of the output isolator was measured to be 1.1 dB. Up to 2.9 W of output signal power (P_S) was obtained with $P_{in} = 4.75$ mW and $P_P = 9$ W, resulting in a fiber-to-fiber gain (G) of 27.9 dB and η of 33.5%. While the simulated P_S at maximum P_P is 8% (0.4 dB) higher than the experimentally measured P_S, the agreement between simulation and data is still good Extrapolating from the data in Fig. 6, we find that 15 W of P_P at 1567 nm will be required to achieve a P_S of 5 W at 1761 nm in the same amplifier configuration.

For P_P above 2 W, the OSNR value at 1761 nm is more than 55 dB in 0.1 nm and remains greater than 35 dB in 0.1 nm with respect to the peak ASE power. The fraction of the total output power emitted as ASE decreases from 20% at low pump power level to less than 10% at 9 W of P_P. Also, we measured that the residual pump at the amplifier output contributes less than 2% of the total power over the entire pump power range. We find that in all of our measurements, the measured OSNR is consistent with the simulated and measured noise figure values.

A typical measured output spectrum, displayed in red in Fig. 7 for a P_P of 9 W. The atmospheric water absorption lines do not significantly affect the measurement of the signal. Due to the co-pumped architecture of the booster stage amplifier, about 60 mW of residual pump power is present at the amplifier output. This residual pump can be filtered out by a low loss bandpass filter in applications where pump feedthrough could be detrimental to the operation of a fiber optic system. The simulated spectrum, represented by the blue dashed curve, shows a good agreement with the measurements, with the exception of the long-wave regime (1850–1950 nm) where it predicts higher ASE levels. We attribute this discrepancy to the expected wavelength dependence of the optical transmission, $T_{WDM}(\lambda) = \sin^2\{\pi(\lambda_1 - \lambda)/[2(\lambda_1 - \lambda_2)]\}$, of the fused fiber WDMs which was not included in the simulations. Here the WDMs used were designed to separate the wavelengths $\lambda_1 = 1760$ nm and $\lambda_2 = 1567$ nm.

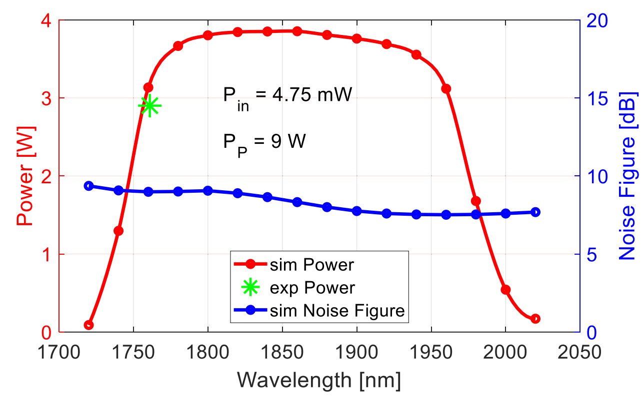

Fig. 8. Simulated output powers (red, left axis) and noise figures (blue, right axis) of the two-stage TDFA as a function of signal wavelength. Experimentally measured power is marked with a green asterisk.

Fig. 7 also shows the simulated output spectrum, represented by the black dashed curve, for the two-stage TDFA with a 1-nm-wide (FWHM) interstage bandpass filter (see Fig. 1). For this configuration, the total output ASE power is <0.2 mW, which corresponds to a reduction of 25 dB in broadband output spontaneous power when using the interstage bandpass filter.

Simulations of the output power (P_S) vs. signal wavelength (λ_S), plotted in red in Fig. 8, show that the 3 dB (50%) output power bandwidth of the two-stage TDFA is from 1745 to 1980 nm or 135 nm. The experimentally measured P_S at 1761 nm is represented on the graph with a green asterisk and agrees quite well with the results of the simulations. Future measurements will study the comparison with simulation over a wider wavelength range. The external noise figure (NF) of the two-stage amplifier, plotted in blue, decreases from is 9.5 to 7.5 dB with increasing signal wavelength. This decreasing NF value is due to the decreasing absorption coefficient as the signal wavelength (see Fig. 2).

Here let us study in detail the dependence of P_S on both λ_S and fiber lengths (F1 and F2) for the two-stage TDFA shown in Fig. 1. As stated in Section II, we chose starting lengths of F1 = 1.0 m and F2 = 1.0 m based on an initial simulation that indicated acceptable target output powers at 1760 nm for our two-stage amplifier. To investigate whether these initial fiber lengths were

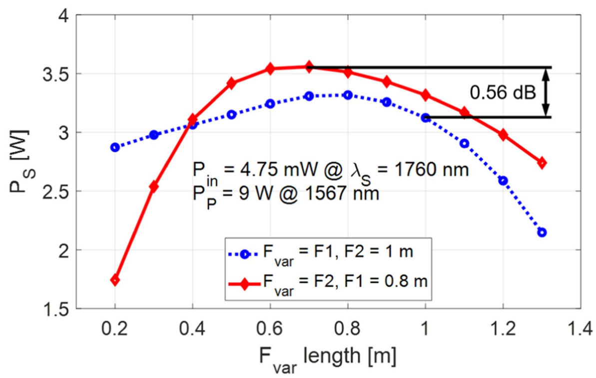

Fig. 9. Dependence of output power (Ps) on active fiber length F1 with F2 = 1.0 m (blue curve), and on active fiber length F2 with F1 = 0.8 m (red curve) for $P_P = 9.0$ W at 1567 nm.

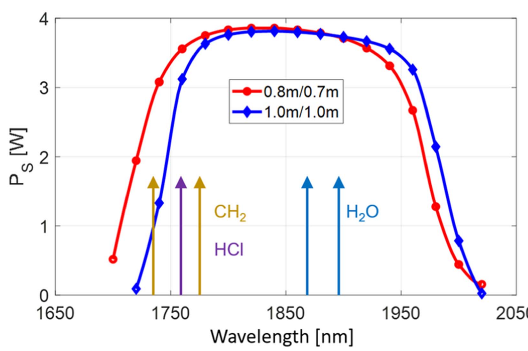

Fig. 10. Comparison of simulated output power (P_S) vs. signal wavelength (λ_S) for F1/F2 lengths of 1.0 m/1.0 m and 0.8 m/0.7 m. Significant in-band molecular absorption lines are indicated by the vertical arrows.

close to optimum values over the full 1760–1960 nm operating spectral range, we subsequently performed a two-part optimization study, first by varying the length of F1 with F2 fixed at its initial value, and then second by varying F2 with the optimized value of F1 in the first part of the study,

For the first part of our optimization study, we plot in Fig. 9 for $P_P = 9$ W the simulated output power (P_S) at 1760 nm as a function of the length of the first stage active fiber F1 while keeping the second stage F2 = 1 m constant (blue curve). We observe that the optimum P_S is reached for F1 = 0.8 m. This optimization of F1 yields an increase in P_S from 3.12 W at 1.0 m to 3.32 W at 0.8 m.

Second, while holding F1 constant at its new optimum value of 0.8 m, we then varied the length of F2 to find its optimum length leading to the maximum P_S. Our simulation results yielded a value of F2 = 0.7 m as shown in Fig. 9 (red curve). The optimization of F2 resulted in Ps = 3.56 W, representing a power increase of 14% (0.56 dB).

Fig. 10 now contrasts the output power (P_S) vs. wavelength (λ_S) of both the initial amplifier design with fiber lengths of F1/F2 = 1 m/1.0 m and the optimized design with F1/F2 = 0.8 m/0.7 m. From Fig. 10 we observe that the optimized design: 1) shifts the bandwidth by 25 nm toward the lower wavelengths, increasing the output power for shorter wavelengths (in particular at 1760 nm), 2) increases the initial 3 dB bandwidth

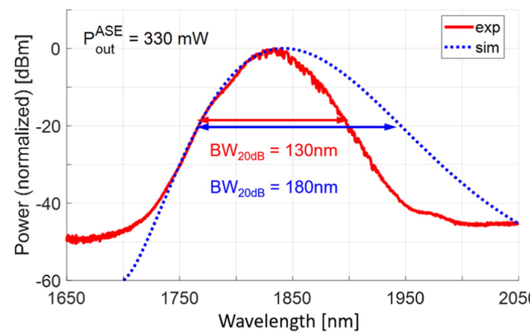

Fig. 11. Spectrum of the two-stage TDFA operated as an ASE source pumped by 1.5 W of 1567 nm pump.

of 230 nm (i.e., 1745–1975 nm) to 245 nm (i.e., 1720–1965 nm) and 3) produces the same peak level of P_S.

Additional simulations not plotted here indicated that fiber lengths shorter than 0.8 m/0.7 m did not shift further the TDFA's bandwidth to lower wavelength range, but exhibited significantly lower output powers. From these results we conclude that 0.8 m/0.7 m represent the optimum F1/F2 lengths for best CW performance of the amplifier in the low wavelength region of its spectrum.

As indicated in Fig. 10, this increase in output powers at the lower wavelengths of 1720–1760 nm is highly desirable for the bio-photonic applications with CH_2 absorptions at 1730 and 1760 nm described above [8], [9], [10] and for the detection of HCl at 1742 nm [22]. In addition, we note that the broadband TDFA exhibits high output power at 1854 and 1877 nm for measurements involving the high sensitivity detection of water vapor [23].

V. ASE Performance of the Two-Stage TDFA

The architecture of the two-stage TDFA allows for operation as a broadband ASE source, as illustrated in Fig. 11. Up to 330 mW of broadband output power has been measured with a P_P of 1.5 W. The 20-dB bandwidth of the ASE source was 130 nm spanning between 1770 and 1900 nm. Similar to the previous results in Fig. 7, the simulations predict an ASE bandwidth that extends 50 nm wider than experiment on the long wavelength side of the spectrum, from 1770 to 1950 nm. Here, we attribute this difference between experiment and simulation to the wavelength dependence of the transmission $T_{WDM}(\lambda)$ of the fused fiber WDMs which was not included in the simulations.

VI. Pulse Performance of the Two-Stage TDFA

Fig. 12 shows the schematic of the pulsed TDFA. In this setup we have operated the preamplifier in a CW mode, and have inserted an acousto-optic modulator (AOM, Gooch and Housego Fiber-Q) after the circulator, so that the input to the booster stage is pulsed. The AOM was originally optimized to operate at 2050 nm with an insertion loss of 2.5 dB, however. in our experiments, it was operated at 1761 nm with 6 dB of insertion losses. The AOM has rise/fall times around 10 ns. The third output of the circulator was used to monitor the onset

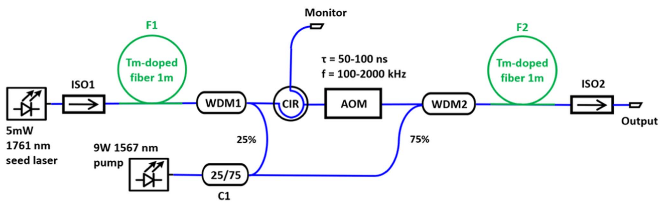

Fig. 12. Optical architecture of the TDFA operated in the pulsed regime.

stimulated Brillouin scattering (SBS) from the power booster. The fiber lengths employed in the pulsed experiments were F1/F2 = 1 m/1 m and might not be an optimal choice for pulsed performance. Further optimization of the F1 and F2 lengths may allow us to improve the results presented here.

In the first series of experiments, the AOM produced square, pulses with $\tau = 50$ ns and pulse repetition frequency (PRF) between 100 kHz and 2 MHz corresponding to the duty cycle (DC) from 0.5 to 10%. Fig. 14(a) shows the measured average signal output power $\overline{P_S}$ (blue, right axis) and the peak signal power P_S^{peak}(red, left axis) for a fixed P_P of 9 W. The signal power is measured within ±1 nm of the signal wavelength of 1761 nm. The peak input power into the second stage is 120 mW. For high DC, $\overline{P_S}$ of more than 2 W can be obtained, which is 73% of the power obtained for CW operation. For DC = 10% the average input power into the booster stage is 12 mW, resulting in 22.5 dB of gain (G) in this stage. With the decrease of PRF, $\overline{P_S}$ decreases and reaches 0.44 W for PRF = 100 kHz. As a result of the decreased DC, the average input power is now only 0.6 mW and the external booster stage gain reaches 28.6 dB. Taking into account the losses of the WDM (0.4 dB) and of the ISO2 (1.1 dB), the small signal gain (G) of the booster stage is more than 30 dB.

With the decrease of the DC, P_S^{peak} increases, as shown by the red points in Fig. 13(a). The increase of P_S^{peak} in the fiber induces nonlinear effects, such modulation instability and SBS. These effects lead to broadening of the signal in the spectral domain and to pulse distortion in the time domain as illustrated in Fig. 13(b) and (c), respectively. The spectra were collected with a Yokogawa AQ6375B optical spectrum analyzer (OSA) and the pulses were recorded using a 12 GHz photodiode (EOT ET-5000F) connected to a 350 MHz oscilloscope (Keysight InfiniVision DSOX3034T).

For PRF > 400 kHz the OSNR remains above 50 dB in 0.1 nm and reaches more than 55 dB in 0.1 nm for PRF > 1 MHz. At the same time, the ASE contributes less than 6% of the total output power. Due to the co-pumped architecture of the power booster, the residual pump contributes less than 20% of the total output power. For PRF < 400 kHz, we observe an onset of the modulation instability, and below 200 kHz the spectrum is broadening towards the long wavelengths as a result of the supercontinuum generation, as shown in Fig. 13(b).

Fig. 13(c) shows that, decreasing the PRF also strongly affects the output pulse shape. Even for the PRF of 1 MHz, pulse distortion due to gain peaking can be observed. Decreasing the PRF to 500 kHz increases the effects of gain peaking, and also results in shortening the pulse length due to gain depletion of

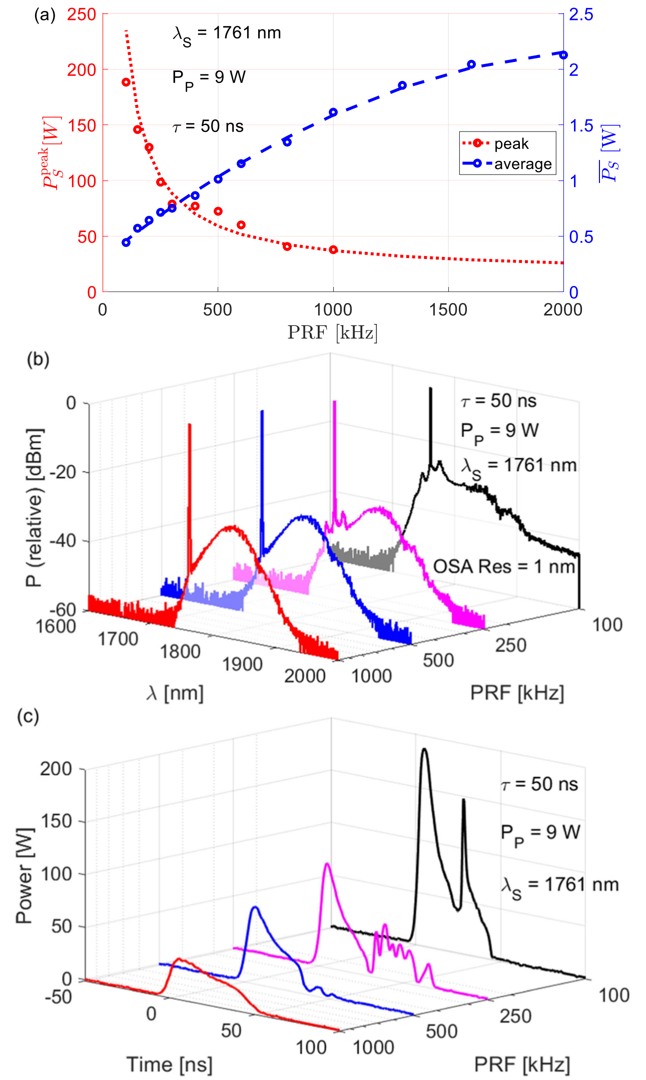

Fig. 13. (a) Average (red, right axis) and peak (blue, left axis) output signal power of the pulsed TDFA as a function of the PRF for fixed pump power of 9 W and pulse duration of 50 ns. (b) And (c) show the corresponding spectra and pulse shapes, respectively.

the fiber. Further decrease of the PRF leads to generation of secondary pulses after the primary pulse, that are responsible for the supercontinuum spectral broadening. The measured pulse shapes are consistent with the pulse shapes obtained in simulations taking into account the SBS [24]. The peak powers measured at the leading edge of the pulse reach 180 W. For PRF < 200 kHz, we have observed a sharp increase of the light intensity at the monitor port, suggesting the onset of SBS.

In order to study the effects of gain peaking, we have decided to work at the PRF > 1 MHz and use a pulse pre-shaping to correct the output pulse shape. The AOM was driven by an arbitrary wave generator (AWG: Rigol DG4162) with 5 ns rise/fall time. The results of these experiments are shown in Figs. 14 and 15.

Fig. 14(a) shows the dependence of the output pulse energy (E) on P_P for two different PRFs: 1 MHz (solid curves) and 2 MHz (dashed curves). At both PRFs, E is measured with square input pulse, (red curves) and with pre-shaping, where the input

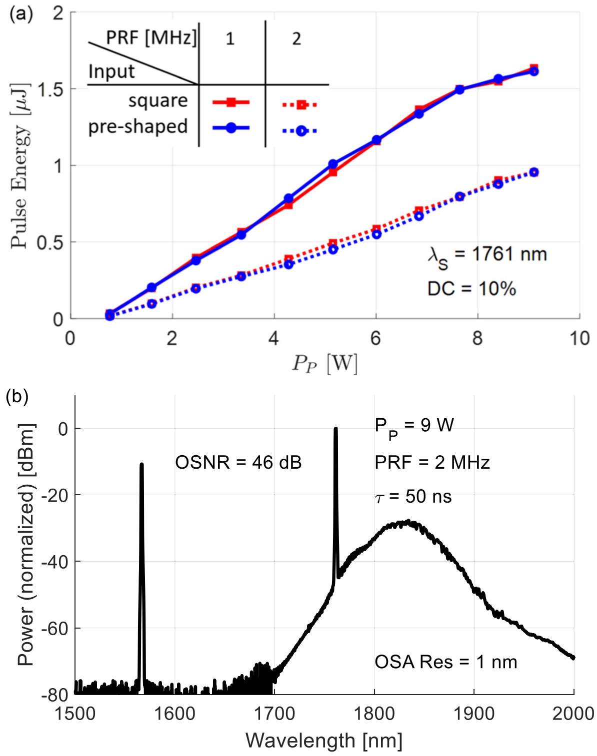

Fig. 14. (a) Pulse energy of the two-stage TDFA vs 1567 nm pump power for the input signal at 1761 nm. (b) Measured output spectra of the pulsed TDFA.

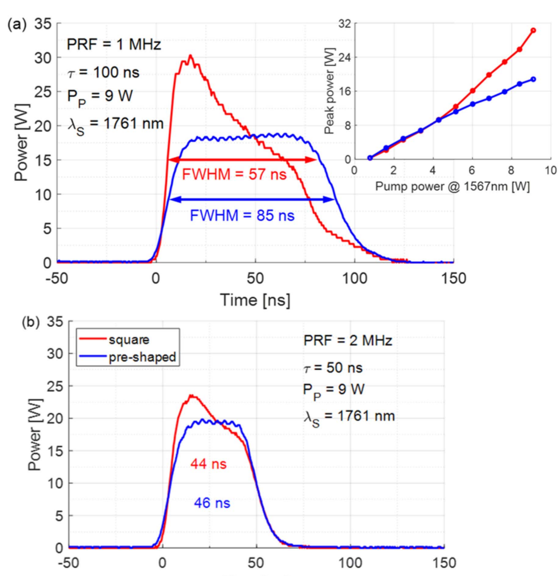

Fig. 15. Output pulse shapes from the pulsed TDFA operated at DC = 10% measured at PRF of 1 MHz (a) 2 MHz (b). The red (blue) curves show the output pulse shapes obtained with a square (pre-shaped) input pulse. The inset in panel (a) shows the evolution of pulse peak power as a function of P_P for PRF of 1 MHZ.

pulse shape is optimized to yield a gain-equalized output pulse for highest pump power, (blue curves). In all the studied cases, the target duty cycle was 10%. Fig.14(a) shows that E with and without pre-shaping are virtually identical. For PRF = 2 MHz, E increases linearly with P_P and reaches 0.95 μJ. for $P_P = 9$ W. In case of PRF = 1 MHz, E increase linearly and ends by a roll off for $P_P > 7.5$ W, and the maximum E reached 1.5 μJ. The maximum available E may be limited by the saturation power of the fiber used and might be increased by using a fiber with a larger core diameter. The measured spectra for all of the cases shown in Fig. 14(a) are very similar, and a typical spectrum at $P_P = 9$ W is shown in Fig. 14(b). For $P_P > 3$ W, the OSNR remains above 54 dB in 0.1 nm. The ratio of the power emitted as ASE (residual pump) to the total power decreases (increases) from 10% (7%) at $P_P = 2$ W to 6% (20%) at $P_P = 9$ W. These results can be improved if a mid-stage narrow band-pass filter at the signal wavelength is introduced.

Fig. 15 shows the output pulse shapes measured at the PRF = 1 MHz (a) and PRF = 2 MHz (b). The pulses measured with a square input pulse (red) are compared with the gain-equalized pulses (blue). For PRF = 1 MHz, the dependence of the P_S^{peak} as a function of P_P is shown in the inset of panel (a). We observe that input pulse pre-shaping allows for efficient gain equalization of the output pulse, especially in the high gain and high output power regimes. In case of the PRF = 1 MHz, P_S^{peak} is reduced from 31 to 19 W by the process of gain-equalization, which reduces the detrimental effects of the nonlinearities triggered by the high peak power levels. Also, the pulse full-width half-maximum (FWHM) of the gain-equalized pulse is closer to the target pulse duration than in the case of the square input pulse. The 5% amplitude oscillation visible on top of the pulse has the oscillation frequency of 200 MHz, which corresponds to the RF frequency or the driver (Gooch and Housego 1250AFP-AD-6.0) used to drive the AOM.

We observe that the output pulses have a smaller rise time than fall time. This phenomenon is caused by a larger gain due to a higher fiber inversion experience by the rising edge of the pulse as compared to the trailing pulse edge.

VII. Discussion

In the pulsed regime, to our knowledge, this work is the first report of ns AWG-pulse-shaped PM TDFAs with multi-Watt level average output powers using a commercially available single-clad fiber with a small core diameter of 5 μm and in-band pumping at 1567 nm. Previous ns pulsed work with single-clad fibers employed non-PM Tm-doped 10-μm fibers pumped at 793 nm, exhibited 1 W average output power at 34 ns pulse width and 5 W average output power at 514 ns pulse width, both at 100 kHz repetition rate [25]. W e observe that the onset of nonlinear effects will be further suppressed by using Tm-doped fibers with somewhat larger core diameters.

Other work on pulsed TDFAs and Tm-doped fiber lasers with nanosecond pulse widths employs large core diameter (20–30 μm) double clad non-PM Tm-doped fibers in the output amplifier stage. For example, Li et al. demonstrated pulse widths of 100 ns and an average output power of 12.5 W at 25 kHz repetition rate with a 25 μm double clad Tm-doped fiber amplifier pumped at 793 nm [26], [27]. This experiment employed pulse shaping with an AWG and also direct source laser modulation and an electro-optic amplitude modulator to shape the input pulse. Wang et al. generated 156 ns pulses at a 1 MHz repetition rate with 105 W average output power, again using a 25 μm core diameter double clad non-PM Tm-doped fiber power amplifier pumped at 793 nm [28].

VIII. Conclusion

We have reported the performance of CW and pulsed single-clad PM Tm-doped fiber amplifiers optimized for the wavelength band from 1760 to 1960 nm. For CW operation, output powers as high as 0.5 W and 3 W were obtained in a single- and two-stage amplifier configurations, respectively, with OSNR higher than 53 dB in 0.1 nm. Optimizing active fiber lengths yielded a 3 dB (50%) output power bandwidth for the amplifier of 1720–1970 nm or 250 nm. Such bandwidth covers many molecular and ionic absorption wavelengths of great practical interest, e.g., 1730 nm, 1742 nm, 1762 nm, 1854 nm, and 1877 nm.

In the pulsed regime, average output powers as high as 2 W in the 50–100 ns pulsed regime, and an OSNR $>$ 55 dB/0.1 nm were achieved. We demonstrated that by pre-shaping the input pulse with an arbitrary waveform generator, we obtained square output pulses with 50–100 ns duration and 10% duty cycle. At 1 MHz and 2 MHz pulse repetition frequencies, the pulse pre-shaping does not affect the pulse energy, but reduces the pulse distortion and minimizes the peak power allowing to effectively suppress fiber nonlinear generation such as stimulated Brillouin scattering (SBS) and modulation instability (MI). For pulse repetition frequencies between 1 and 2 MHz, we have measured up to 20 W of peak power and pulse energies reaching 1.6 μJ. Reduction of the insertion losses of the acousto-optic modulator will lead to higher input power into the booster amplifier stage and a better saturation. Addition of the interstage filter should remove out of band ASE power and prevent an early onset of nonlinearities. Finally, increasing the core size of the single-mode polarization-maintaining thulium-doped fiber will lead to a higher saturation power and therefore a higher output peak power.

We note that our packaged 1760 nm TDFA is pumped with a passively cooled 1567 nm fiber laser, which greatly enhances its areas of practical application.

With its high levels of CW and pulsed performance, our amplifier can be immediately applied in experiments such as biological physics and spectroscopy, selective imaging of lipids and proteins by excitation of CH_2 in the 1730–1760 nm optical window, high sensitivity detection of HCl and water vapor, or mid-IR frequency generation.

In particular, the application of this amplifier to quantum computing applications using the IR resonance at 1762 nm in ^{133}Ba+ ions is of great current interest. This is because of the highly favorable nature of the ^{133}Ba+ ion for many quantum computing operations, and also because the natural linewidth of this 1762 nm transition is only 5 mHz (0.005 Hz) [29], [30]. We anticipate many productive future studies of the quantum noise and phase noise of high performance 1760 nm TDFAs using the narrow linewidth IR transition. This new and significant application to an IR transition in an ion with a 5 mHz natural linewidth will open many new exciting and rewarding horizons in fiber optical amplifier design and quantum noise studies.

References

[1] Z. Li et al., "Diode-pumped wideband thulium-doped fiber amplifiers for optical communications in the 1800–2050 nm window," *Opt. Exp.*, vol. 21, no. 22, pp. 26450–26455, Nov. 2013, doi: 10.1364/OE.21.026450.

[2] J. M. O. Daniel et al., "Ultra-short wavelength operation of a thulium fibre laser in the 1660–1750 nm wavelength band," *Opt. Exp.*, vol. 23, no. 14, pp. 18269–18276, Jul. 2015, doi: 10.1364/OE.23.018269.

[3] Z. Li et al., "Exploiting the short wavelength gain of silica-based thulium-doped fiber amplifiers," *Opt. Lett.*, vol. 41, no. 10, pp. 2197–2200, Dec. 2016, doi: 10.1364/OL.41.002197.

[4] S. Chen et al., "Ultra-short wavelength operation of thulium-doped fiber amplifiers and lasers," *Opt. Exp.*, vol. 27, no. 25, pp. 36699–36707, Dec. 2019, doi: 10.1364/OE.27.036699.

[5] C. Romano, R. E. Tench, and J.-M. Delavaux, "Simulation of 2 μm single clad thulium-doped silica fiber amplifiers by characterization of the $^3F_4$–$^3H_6$ transition," *Opt. Exp.*, vol. 26, no. 20, pp. 26080–26092, Oct. 2018, doi: 10.1364/OE.26.026080.

[6] R. E. Tench, C. Romano, and J.-M. Delavaux, "Broadband 2-W output power tandem thulium-doped single clad fiber amplifier at 2 μm," *IEEE Photon. Technol. Lett.*, vol. 30, no. 5, pp. 503–506, Mar. 2018, doi: 10.1109/LPT.2018.2801840.

[7] R. E. Tench et al., "Experimental performance of a broadband dual-stage 1950 nm PM single-clad Tm-doped fiber amplifier," *IEEE Photon. Technol. Lett.*, vol. 32, no. 15, pp. 956–959, Aug. 2020, doi: 10.1109/LPT.2020.3006697.

[8] P. Wang et al., "Bond-selective imaging of deep tissue through the optical window between 1600 and 1850 nm," *J. Biophoton.*, vol. 5, no. 1, pp. 25–32, Jan. 2012, doi: 10.1002/jbio.201100102.

[9] L. Wang et al., "Tapered fiber-based intravascular photoacoustic endoscopy for high-resolution and deep-penetration imaging of lipid-rich plaque," *Opt. Exp.*, vol. 27, no. 9, pp. 12832–12840, Apr. 2019, doi: 10.1364/OE.27.012832.

[10] J. T. Friedlein et al., "Dual-comb photoacoustic spectroscopy," *Nature Commun.*, vol. 11, Jun. 2020, Art. no. 3152, doi: 10.1038/s41467-020-16917-y.

[11] L. Yang et al., "30-W supercontinuum generation based on ZBLAN fiber in an all-fiber configuration," *Photon. Res.*, vol. 7, no. 9, pp. 1061–1065, Sep. 2019, doi: 10.1364/PRJ.7.001061.

[12] M. H. M. Shamim, I. Alamgir, and M. Rochette, "High efficiency Raman soliton generation in passive silica fiber," in *Proc. Conf. Lasers Electro-Opt. Europe Eur. Quantum Electron. Conf.*, Munich, Germany, 2021, p. 1, doi: 10.1109/CLEO/Europe-EQEC52157.2021.9541901.

[13] W. Walasik, D. Traoré, A. Amavigan, R. E. Tench, J. -M. Delavaux, and E. Pinsard, "2-μm narrow linewidth all-fiber DFB fiber Bragg grating lasers for Ho- and Tm-doped fiber-amplifier applications," *J. Lightw. Technol.*, vol. 39, no. 15, pp. 5096–5102, Aug. 2021, doi: 10.1109/JLT.2021.3079235.

[14] W. Walasik, R. E. Tench, G. Rivas, J. -M. Delavaux, and I. Farley, "1760 nm multi-watt broadband PM Tm-doped fiber amplifier," in *Proc. Conf. Lasers Electro-Opt.*, May 2022, pp. 1–2.

[15] W. Walasik, R. E. Tench, G. Rivas, J. -M. Delavaux, and I. Farley, "1760 nm multi-watt broadband PM CW and pulsed Tm-doped fibre amplifier," in *Proc. Eur. Conf. Opt. Commun.*, Sep. 2022, pp. 1–4.

[16] D. Y. Shen, J. K. Sahu, and W. A. Clarkson, "High-power widely tunable Tm: Fibre lasers pumped by an Er,Yb co-doped fibre laser at 1.6 μm," *Opt. Exp.*, vol. 14, no. 13, pp. 6084–6090, Jun. 2006, doi: 10.1364/OE.14.006084.

[17] Z. Quan et al., "400 mW narrow-linewidth Tm-doped silica fiber laser output near 1750 nm with volume Bragg grating," *Sci. Rep.*, vol. 5, Jul. 2015, Art. no. 12034, doi: 10.1038/srep12034.

[18] M. D. Burns, P. C. Shardlow, P. Barua, T. L. Jefferson-Brain, J. K. Sahu, and W. A. Clarkson, "47 W continuous-wave 1726 nm thulium fiber laser core-pumped by an erbium fiber laser," *Opt. Lett.*, vol. 44, no. 21, pp. 5230–5233, Oct. 2019, doi: 10.1364/OL.44.005230.

[19] L. Zhang, J. Zhang, Q. Sheng, C. Shi, W. Shi, and J. Yao, "Watt-level 1.7-μm single-frequency thulium-doped fiber oscillator," *Opt. Exp.*, vol. 29, no. 17, pp. 27048–27056, Aug. 2021, doi: 10.1364/OE.434001.

[20] E. Desurvire, *Erbium-Doped Fiber Amplifiers: Principles and Applications*, 1st ed. Hoboken, NJ, USA: Wiley, 1994.

[21] C. R. Giles, C. A. Burrus, D. J. DiGiovanni, N. K. Dutta, and G. Raybon, "Characterization of erbium-doped fibers and application to modeling 980-nm and 1480-nm pumped amplifiers," *IEEE Photon. Technol. Lett.*, vol. 3, no. 4, pp. 363–365, Apr. 1991, doi: 10.1109/68.82113.

[22] E. A. Curtis, N. C. G. Black, G. S. Walsh, C. G. Lucas, and G. P. Barwood, "Ultra-sensitive, real-time detection of HCl using a transportable NICE-OHMS system," in *Proc. IEEE Conf. Lasers Electro-Opt.*, 2021, pp. 1–2, doi: 10.1364/CLEO_AT.2021.JTh3A.43.

[23] A. Khan et al., "Low power greenhouse gas sensors for unmanned aerial vehicles," *Remote Sens.*, vol. 4, no. 5, pp. 1355–1368, May 2012, doi: 10.3390/rs4051355.

[24] G. Kulscar, Y. Jaouën, G. Canat, E. Olmedo, and G. Debarge, "Multiple-stokes stimulated Brillouin scattering generation in pulsed high-power double-cladding Er^{3+}–Yb^{3+} codoped fiber amplifier," *IEEE Photon. Technol. Lett.*, vol. 15, no. 6, pp. 801–803, Jun. 2003, doi: 10.1109/LPT.2003.811141.

[25] A. Sincore, N. Bodnar, J. Bradford, A. Abdulfattah, L. Shah, and M. C. Richardson, "SBS threshold dependence on pulse duration in a 2053 nm single-mode fiber amplifier," *IEEE J. Lightw. Technol.*, vol. 35, no. 18, pp. 4000–4003, Sep. 2017, doi: 10.1109/JLT.2017.2729508.

[26] Z. Li et al., "High-energy diode-seeded nanosecond 2 μm fiber MOPA systems incorporating active pulse shaping," *Opt. Lett.*, vol. 39, no. 6, pp. 1569–1572, Mar. 2014, doi: 10.1364/OL.39.001569.

[27] A. M. Heidt, Z. Li, and D. J. Richardson, "High power diode-seeded fiber amplifiers at 2 μm—From architectures to applications," *IEEE J. Sel. Topics Quantum Electron.*, vol. 20, no. 5, pp. 525–536, Sep./Oct. 2014, doi: 10.1109/JSTQE.2014.2312933.

[28] X. Wang et al., "105 W ultra-narrowband nanosecond pulsed laser at 2 μm based on monolithic Tm-doped fiber MOPA," *Opt. Exp.*, vol. 23, no. 4, pp. 4233–4241, Feb. 2015, doi: 10.1364/OE.23.004233.

[29] A. A. Graps, "From perfect qubit to goldilocks qubit for ion traps," IQT News, 2022. [Online]. Available: https://www.insidequantumtechnology.com/news-archive/from-perfect-qubit-to-goldilocks-qubit-for-ion-traps/

[30] C. D. Bruzewicz et al., "Trapped-ion quantum computing: Progress and challenges," *Appl. Phys. Rev.*, vol. 6, 2019, Art. no. 021314, doi: 10.1063/1.5088164.

[31] J. Mirza et al., "Design of an efficient thulium-doped fiber amplifier for dual-hop earth to satellite optical links," *Ain Shams Eng. J.*, vol. 14 no. 7, 2022, Art. no. 101893, doi: 10.1016/j.asej.2022.101893.

[32] [Online]. Available: https://precilasers.com/web/viewer.html?file=..//en/upfiles/file/p18.pdf